6. SPRAY COMBUSTION

6.1 Ignition and Combustion Models

The ignition delay is an important parameter in the operation of diesel engines since it influences hydrocarbon and NO_x emissions. During the delay period, the injected fuel undergoes complex physical and chemical processes such as atomization, evaporation, mixing and preliminary chemical reaction. Ignition takes place after the preparation and reaction of the fuel-air mixture and leads to fast exothermic reaction. The multistep 'Shell' ignition model has been developed for the autoignition of hydrocarbon fuels at high pressures and temperatures by Halstead et al. (1977). The model accounts for multistage ignition and "negative temperature" coefficient phenomena. The model has been applied to diesel combustion by Kong and Reitz (1993).

The reactions and species involved in this kinetic model are as follows:

$RH + O_2$	$\rightarrow$	$2R^*$	K_q	(a)
R^*	$\rightarrow$	$R^* + P + Heat$	K_p	(b)
R^*	$\rightarrow$	$R^* + B$	$f_1 K_p$	(c)
R^*	$\rightarrow$	$R^* + Q$	$f_4 K_p$	(d)
$R^* + Q$	$\rightarrow$	$R^* + B$	$f_2 K_p$	(e)
B	$\rightarrow$	$2R^*$	K_b	(f)
R^*	$\rightarrow$	termination	$f_3 K_p$	(g)
$2R^*$	$\rightarrow$	termination	K_t	(h) (6.1)

where *RH* is the hydrocarbon fuel (C_nH_{2m}), *R** is the radical formed from the fuel, *B* is the branching agent, *Q* is a labile intermediate species, and *P* is oxidized products, consisting of *CO*, CO_2, and H_2O in specified proportions. The expressions for K_q, K_p, K_b, K_t, f_1, f_2, f_3, f_4 etc. are those given by Halstead et al. (1977). In addition, the local concentrations of O_2 and N_2 are needed to compute the reaction rates.

The premise of the Shell model is that degenerate branching plays an important role in determining the cool flame and two-stage ignition phenomena that are observed during the autoignition of hydrocarbon fuels. A chain-propagation cycle is formulated to describe the history of the branching agent, Eqs. (6.1b-f), together with one initiation, Eq. (6.1a), and two termination

reaction, Eqs. (6.1g-h). Some interpretations of these generic species have been proposed. The branching agent *B* is related to hydroperoxides (RO_2H) at low temperatures and to hydrogen peroxides (H_2O_2) at high temperatures. The intermediate species *Q* is related to aldehydes (*RCHO*) during the first induction period and to the alkylperoxy radical (HO_2) and its isomerization products during the second induction period. The formation of intermediate species (Eq. (6.1d)) is the crucial reaction leading to the production of branching agent, which in turn induces hot ignition. The Shell model specifies different values for the kinetic parameters of this reaction for different fuels, and values are given by Kong et al. (1995).

Figure 6.1 shows a comparison between spray ignition experiments and computations of ignition delay times using the Shell model (Kong and Reitz, 1993). The experiments were conducted in a constant volume bomb by Edwards et al. (1992), and used diesel fuel (simulated in the computations as hexadecane) injected into compressed air at 30 atmospheres and 1070 K. Good levels of agreement between measured and predicted ignition delay times are seen over a wide range of operating conditions.

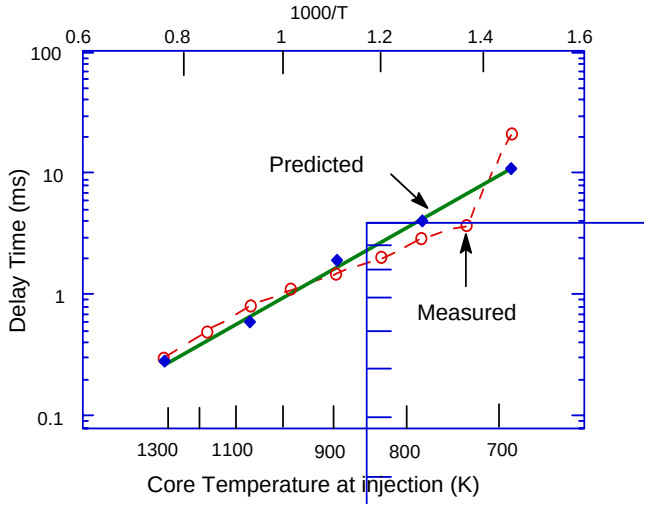

Fig 6.1 Comparison of measured and predicted ignition delay times for constant volume bomb at different chamber gas temperatures.

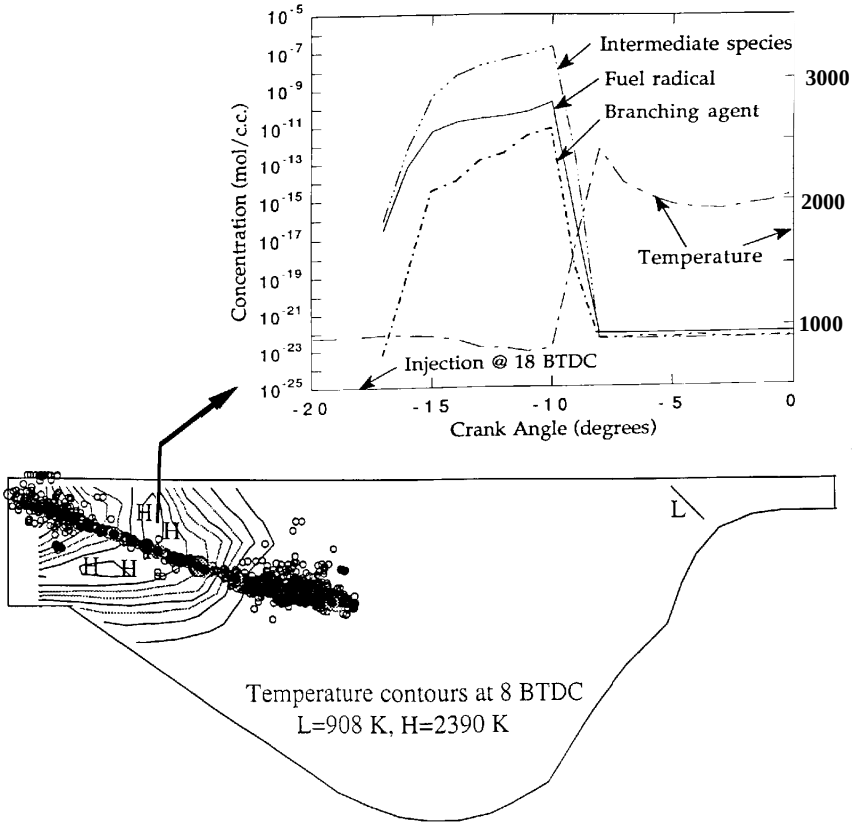

Fig. 6.2 Predicted spray drop locations and temperature contours in a Cummins engine at 8 degrees BTDC. Inset plot shows variation of gas temperature and ignition species concentrations with crank angle in the ignition cell (Kong and Reitz, 1993).

Details of the predicted location and time-history of the ignition process in a Cummins diesel engine are summarized in Fig. 6.2 (Kong and Reitz, 1993). Fuel injection started at 18 degrees BTDC. Ignition takes place some distance downstream of the nozzle at the spray edge at about 9 degrees BTDC. This is evidenced by the high temperature contours which are seen to surround the spray. The build-up and subsequent rapid consumption of the intermediate, branching and radical species that control the ignition process are also shown as a function of crank angle in the ignition cell in Fig. 6.2. After the ignition, the gas temperature variation in the ignition cell reflects the balance between the energy released due to combustion and the energy required to vaporize the liquid fuel.

In practical combustors, once ignition has occurred, the majority of combustion is thought to be mixing-controlled, and the interactions between

turbulence and chemical reactions have to be considered. Several turbulent combustion models which include the effects of turbulence on mean reaction rates are available for engine applications (Magnussen and Hjertager, 1976; Marble and Broadwell, 1977). Based on the fact that the k-ε model is used for turbulence modeling, these combustion models formulate the combustion timescale by making use of the turbulent kinetic energy and its dissipation rate.

The combustion model of Magnussen and Hjertager (1976) is an eddy-dissipation model which assumes a one-step reaction where the fuel or reactive species and oxidizer react at a rate

$$Rate = \mathrm{A}\,(\varepsilon/\mathrm{k})\,Min\left(C_f\,,\ \frac{C_{O2}}{r}\,,\ \mathrm{B}\frac{C_P}{1+r}\right) \qquad (6.2)$$

where A and B are model constants which depend on both the structure of the flame and the reaction between the fuel and oxygen, C_f , C_{O2} and C_P are the concentrations of fuel, oxygen and products, respectively, and r is the stoichiometric mass ratio of oxygen to fuel. One difficulty with the application of one-step models is that r is generally not known a priori in cases of incomplete combustion, as is discussed by Reitz and Bracco (1983).

The coherent flame model of Marble and Broadwell (1977) considers local laminar flamelets stretched by the turbulent flow. The reaction rate is formulated as the product of the flamelet area per unit volume (which is obtained from an additional transport equation for the flame surface density which incorporates the transport, diffusion, production and destruction of flame area) and the local strained laminar flame speed. This class of flamelet models has been used for engine combustion by Dillies et al. (1993).

A simpler combustion model is the laminar-and-turbulent characteristic-time combustion model of Reitz and Bracco (1982), which was applied to engine combustion by Abraham et al. (1985). This model also uses the eddy-breakup concept and has been demonstrated to perform well in various engine applications when combined with the Shell ignition model (e.g., Patterson et al., 1993). The time rate of change of the partial density of species m, due to conversion from one chemical species to another, is given by

$$\frac{d\mathrm{Y}_m}{d\,\mathrm{t}} = -\frac{\mathrm{Y}_m - \mathrm{Y}_m^*}{\tau_c} \qquad (6.3)$$

where Y_m is the mass fraction of species m, Y_m^* is the local and instantaneous thermodynamic equilibrium value of the mass fraction, and τ_c is the characteristic time for the achievement of equilibrium. τ_c is assumed to be the same for the seven species necessary to predict thermodynamic equilibrium temperatures accurately: fuel, viz. O_2, N_2, CO_2, CO, H_2, and H_2O. Among these seven species, six reactive species (i.e., all except N_2) are accounted for in order to solve the local and instantaneous thermodynamic equilibrium values Y_m^*. Since no one-step reaction is assumed, no assumptions about the stoichiometric coefficients is needed.

The characteristic time, τ_c, is assumed to be the sum of a laminar timescale and a turbulent timescale, such that the longer of the two timescales controls the combustion rate. The laminar timescale is of Arrhenius form, and the turbulent timescale is assumed to be proportional to the eddy turnover time, ε/k, similar to the Magnussen and Hjertager (1976) model.

The chemical source term in the species Eq. (2.11) and the chemical heat release in the energy equation (2.15) are found from

$$\Delta\rho_m = -\rho\left(Y_m - Y_m^*\right)\left(1 - e^{-\Delta t/\tau_c}\right) \tag{6.4}$$

$$\Delta Q = -\sum_m \frac{\Delta\rho_m}{W_m}\left(\Delta h_f^0\right)_m \tag{6.5}$$

where Δt is the numerical timestep, and $\dot{\rho}_m^c = \Delta\rho_m/\Delta t$ and $\dot{Q}^c = \Delta Q/\Delta t$. Further details of the combustion model are given by Kong and Reitz (1995).

6.2 Application - Diesel Emissions Modeling

An integrated numerical model has been developed for diesel engine computations based on the KIVA-II code, as described by Patterson et al. (1994) and Kong et al. (1994). Improved submodels include heat transfer, crevice flow, spray, ignition, combustion, soot and NOx emission models. Detailed comparisons between measured and predicted engine performance, and soot and nitric oxide (NOx) emissions have been made, and the predicted results have been found to be in good agreement with the experiments, indicating that computer models are now available to the engine industry for use as predictive design tools.

The computational results were compared with engine experiments performed on a single-cylinder version of the Caterpillar 3406 engine that features state-of-the-art high pressure electronic fuel injection and emissions instrumentation. The engine specifications and operating conditions are given in Table 6.1. The injection pressure was 90 MPa and the nozzle tip had 6 holes with hole diameters of 0.259 mm. Various injection timings and injection schedules (including various injection rates and split injections) have been studied in the experiments (Nehmer and Reitz, 1994).

Table 6.1 Engine Specifications

	Caterpillar	*Tacom*
Bore	137.19 mm	114.3 mm
Stroke	165.1 mm	114.3 mm
Connection rod	261.62 mm	228.6 mm
Displacement	2.44 L	1.173 L
Compression ratio	15.0	16.0
Engine speed	1600 rpm	1500 rpm
Intake pressure	1.82 atm	1.81 atm
Intake temperature	36 C	60 C
Exhaust back pressure	1.57 atm	1.94 atm
Equivalence ratio	0.46	0.5; 0.3
Injection timing (atdc)	-15,-13,-11,-8,-5	-10.5 deg

The model was also applied to a Tacom diesel engine also described in Table 6.1. This engine was utilized to measure time-resolved NO formation by dumping the cylinder mixture at designated crank angles (Donahue, 1993).

The "blob" atomization model (see Section 3.3) was used because it removes the need to specify an assumed initial drop size distribution at the nozzle. The recommended values of the constants for diesel spray computations were used (i.e., B_0 = 0.61 and B_1 = 30, Kong et al. 1995). However, enhanced breakup of drops that impinge on the piston surface was modeled by using B_1=1.73 for those drops, as described in Section 5.3. The drop drag submodel that accounts for the effects of drop distortion and oscillation was used, as described in Section 4.2.

The Shell multistep ignition kinetics model was used to simulate the low temperature chemistry during ignition delay period, as described in Section 6.1. The model is used whenever and wherever the local temperature is lower than 1000K. The laminar-and-turbulent characteristic-time combustion model was used for modeling high temperature combustion.

The extended Zeldovich mechanism described by Heywood (1976) was implemented for predicting NOx formation. The soot emission model used a modified version of the formation model of Hiroyasu and Nishida (1989), and the Nagle and Strickland-Constable (1962) soot oxidation model.

Computations were made considering only one of the six spray plumes by assuming sector symmetry in the engine, as shown in Fig. 3.13. Figure 6.3 shows computed results for a single injection case with injection timing for best BSFC (11 degrees BTDC). The plots show computed temperature contours in the midplane of spray together with spray drop locations in the combustion chamber at 3 and 4 degrees BTDC when ignition occurs. The flame extends back to the injector nozzle and there is significant impingement of the spray on the piston.

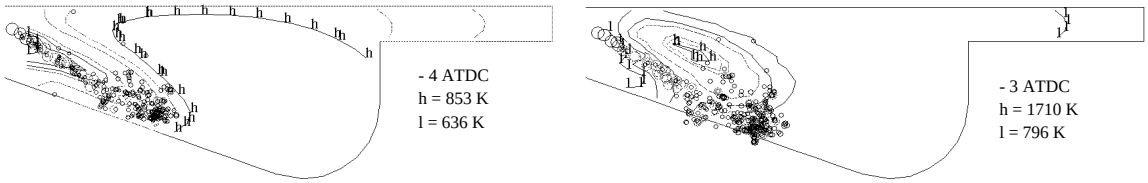

Fig. 6.3 Computed temperature contours and spray distribution in the Caterpillar engine showing ignition (Kong et al., 1994).

The corresponding predicted cylinder pressure variation versus crank angle is shown in Fig. 6.4a, and the predicted and measured apparent rate of heat release is shown in Fig. 6.4b. It is seen that there is excellent agreement between the predicted (labeled 'Present') and measured cylinder pressure and heat release data.

Figure 6.4a also shows computations made using the 'standard' KIVA-II with a one-step Arrhenius combustion model that does not account for the effect of turbulence on combustion. It is seen that the combustion is predicted to be too fast initially. The spray penetration is underpredicted, and rich regions of vaporized fuel are found near the injector nozzle. This trend leads to the large discrepancy between the measured and predicted cylinder pressures which is seen during the power stroke.

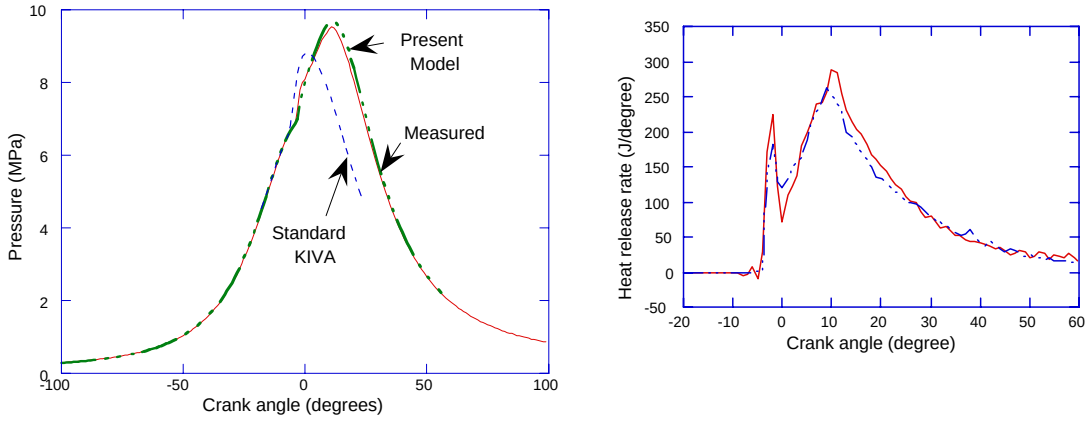

(a.) (b.)

Fig. 6.4 Computed and measured (solid line) a.) cylinder pressures, and b.) heat release rates for Caterpillar engine (Kong et al., 1995).

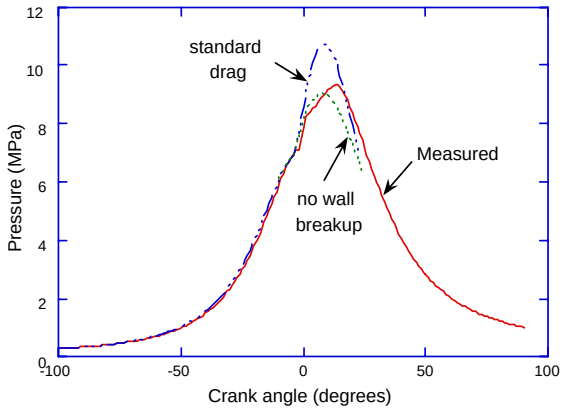

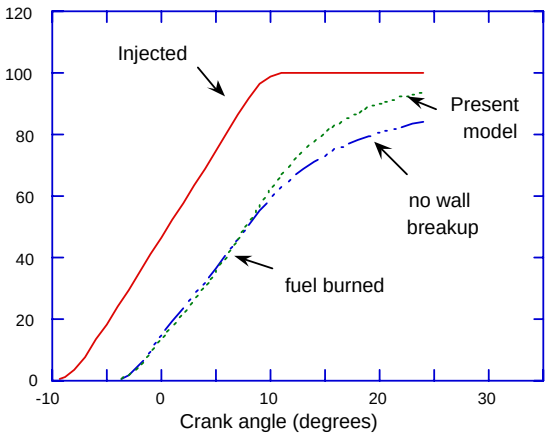

Fig. 6.5 (a.) Effect of drop drag and wall impingement on combustion predictions.

(b.) Effect of enhanced atomization during wall impingement on combustion.

The curve labeled 'Standard drag' in Fig. 6.5a shows that the use of the spherical-drop drag coefficient that does not account for drop distortion, leads to an overestimate in the peak pressure. The reason for this is that the relative velocity between the drop and the gas is higher than in the corresponding dynamically varying drag coefficient computation. This produces smaller breakup drop sizes and these small drops vaporize too fast. This again leads to fast combustion and poor spray penetration, as evidenced by the fact that the predicted cylinder pressures underestimate the measured data during the later part of the power stroke.

Figure 6.5b shows results obtained without modifying the breakup model time constant after drops impact on the piston surface (labeled no wall breakup). In this case liquid and vapor fuel was found to accumulate near the cold piston surface at the bottom of the bowl which does not participate in the combustion process. Figure 6.5b shows that significant unburned fuel remains in the chamber after the combustion stops when wall breakup is not accounted for.

The predicted results have also been compared with in-cylinder flame visualization images by Kong et al. (1995b). This study is useful since it also addresses the local details of combustion predictions, not just the global details as represented by cylinder pressure data. The experimental visualization images were obtained by replacing one of the engine's two exhaust valves with an AVL endoscope system, as shown in Fig. 6.6a. The images shown in Fig. 6.6b show that flames enter the squish region at around 5 or 6 degrees ATDC. The corresponding computational results presented in Fig. 6.6c show that this feature is also predicted by the model since high temperatures are found in the squish region at 10 degrees ATDC.

The location of the high temperature region was found to be sensitive to the details of the turbulence model used in the computations. The modified RNG k-ε model of Han and Reitz (1995) was used for the results given in Fig. 6.6c. Other results obtained using the standard k-ε turbulence model, Eqs. (2.17 and 2.18), did not agree as well with the visualization images, as discussed by Kong et al., (1995).

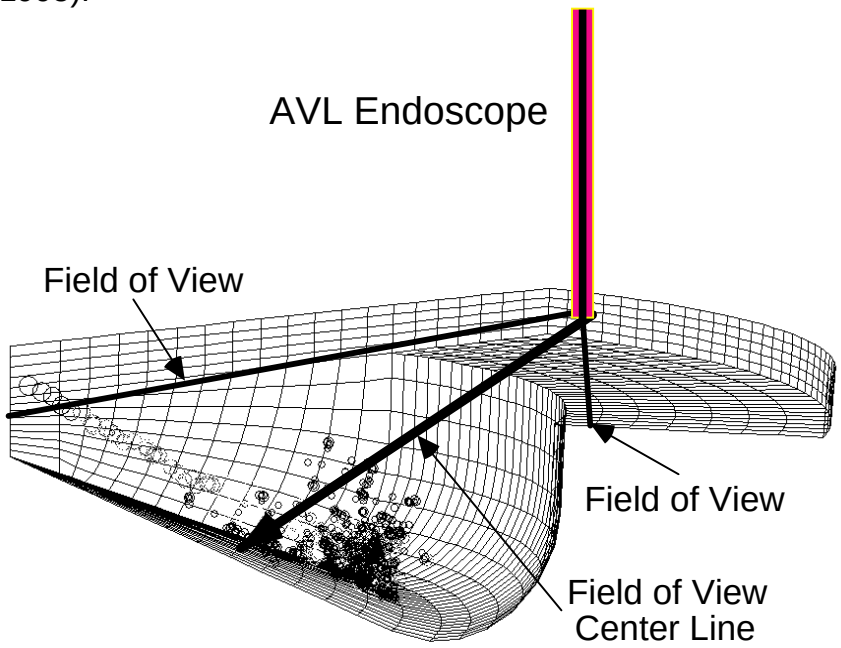

Fig. 6.6a Details of field of view used in the combustion visualization study of Kong et al. 1995b.

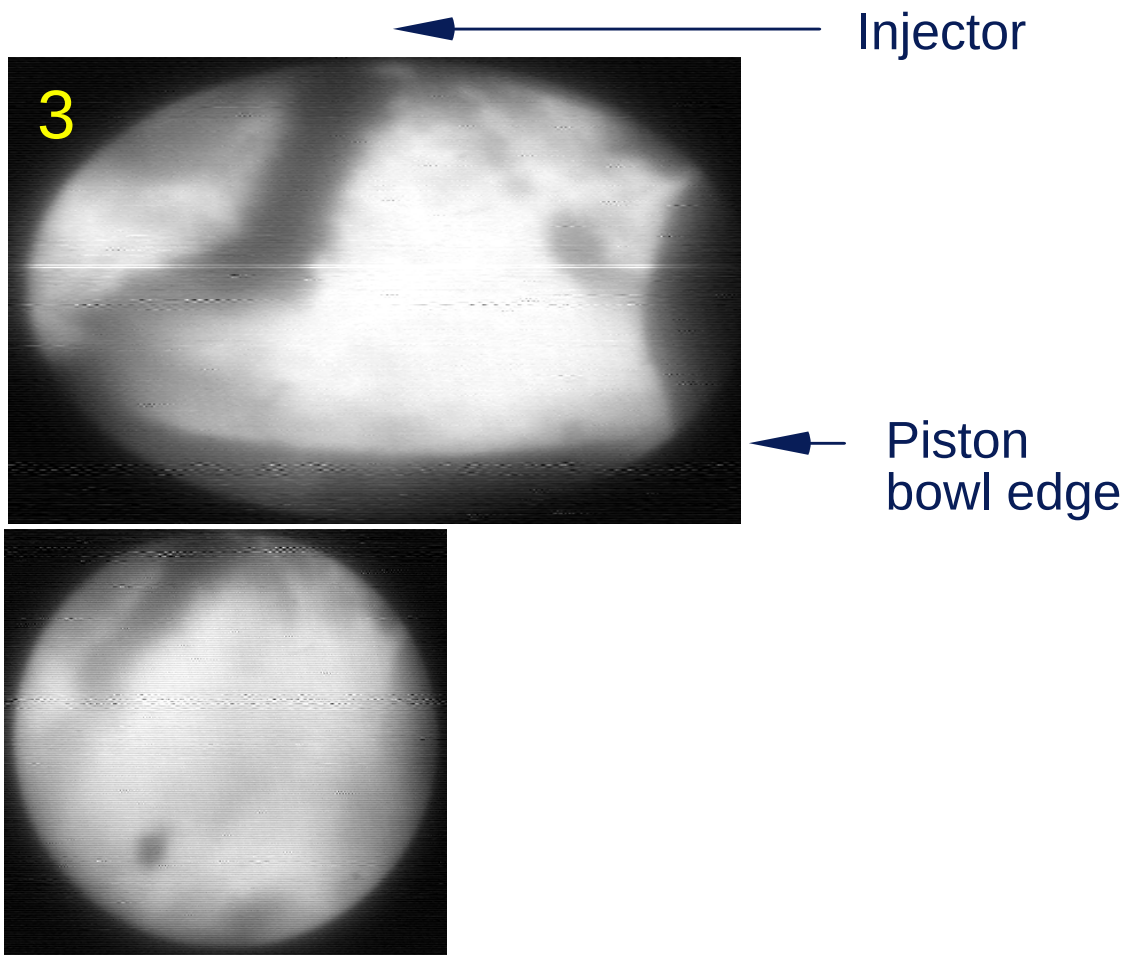

Fig. 6.6b Combustion visualization images at 3 (left) and 6 (right) degrees ATDC showing flames entering the squish region (at the bottom of each frame).

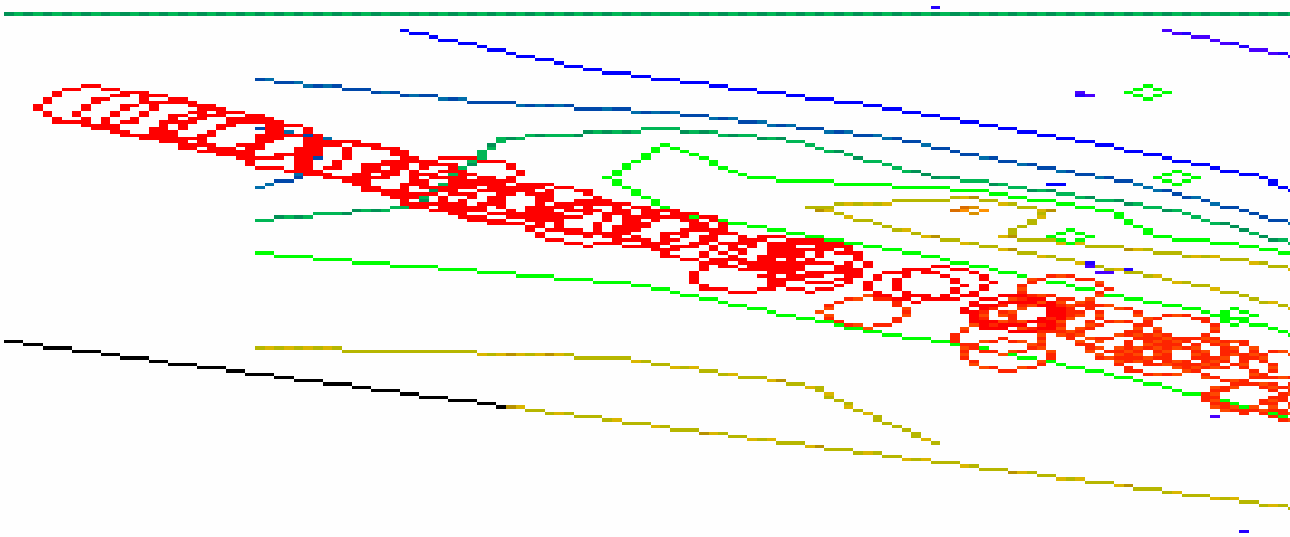

Fig. 6.6c Predicted temperature field in the plane of the spray showing combustion in the squish region by 10 degrees ATDC (Kong et al., 1995)

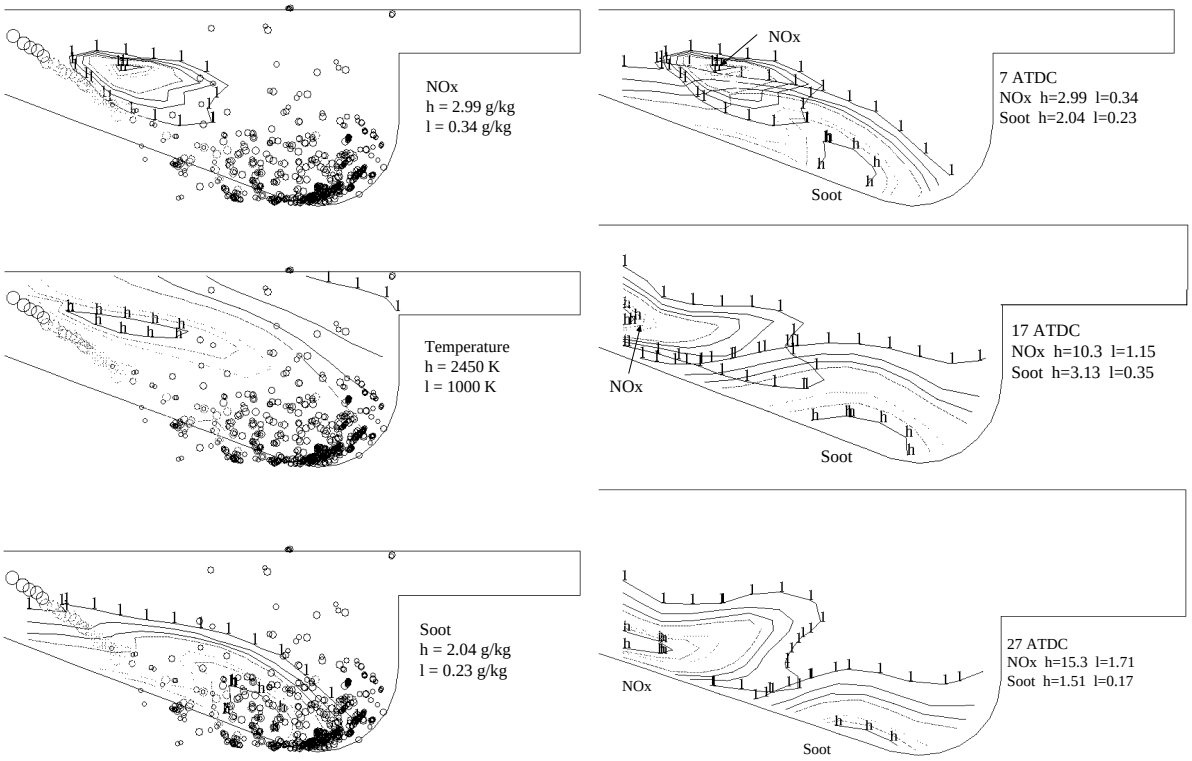

Fig. 6.7 (a.) Predicted spray drop locations, temperature, NOx and soot mass fraction at 7 ATDC.

(b.) Predicted soot and NOx mass fraction (in g/kg-mixture) as a function of crank angle.

Computations have also been made of soot and NOx distributions in the engine. Figure 6.7a shows predicted spray drop locations together with NOx mass fraction, temperature and soot mass fraction contours in the engine at 7 degrees ATDC. NOx is highest in the region where the ignition occurred and the gas has been exposed to high temperatures for the longest time. Soot concentrations are the highest in the rich regions of the spray near the cool piston surface. The time evolution of the soot and NOx distributions is shown in Fig. 6.7b at 7, 17 and 27 degrees ATDC. The majority of the soot is located near the bottom of the bowl, while the NOx is located closer to the injector. Note that the NOx mass fraction high contour values increase significantly (an order of magnitude) while the soot mass fraction increases and then decreases due to oxidation during the period shown in Fig. 6.7b.

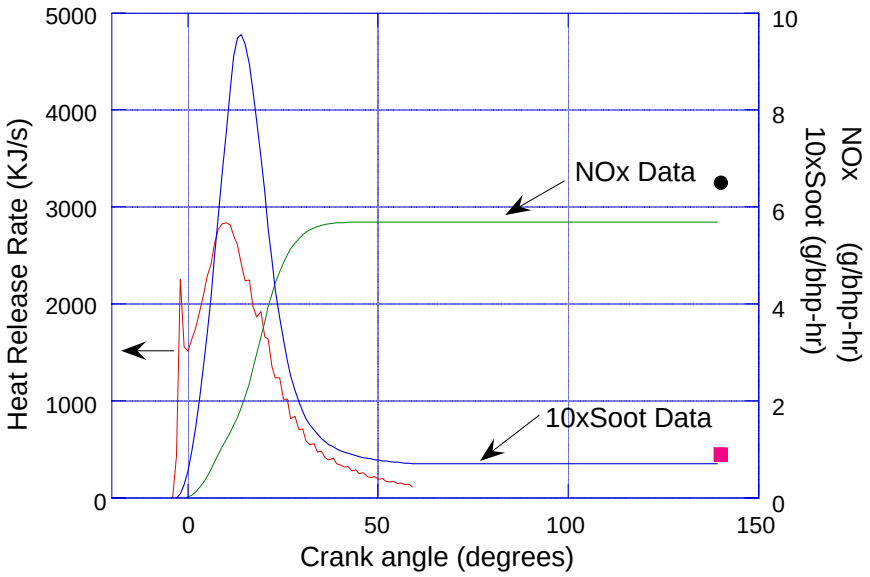

Fig. 6.8 Predicted and measured (exhaust-out at 140 ATDC) NOx and soot data for the -11 atdc injection case. Computed heat release rate curve is also shown for comparison (Kong et al., 1994).

The results of Fig. 6.7b are summarized in Fig. 6.8 which shows the total cylinder soot and NOx variation with crank angle together with the predicted heat release curve for reference. Most of the NOx is predicted to be produced after the peak heat release (i.e., after peak cylinder pressure). During this time soot oxidation accounts for the decrease in the in-cylinder soot levels. Figure 6.8 also allows a comparison between the predicted and measured engine-out soot and NOx values. The predicted soot and NOx data are seen to agree very well with the measured data.

Computations have also been performed for other cases considered in the experiments, including single injection cases at different injection timings (5, 8, 11, 13 and 15 degrees before TDC). The agreement between the measured and predicted cylinder pressures shown in Fig. 6.9 is seen to be very encouraging. However, the measured cylinder pressure data are somewhat over-predicted for the early injection timing cases.

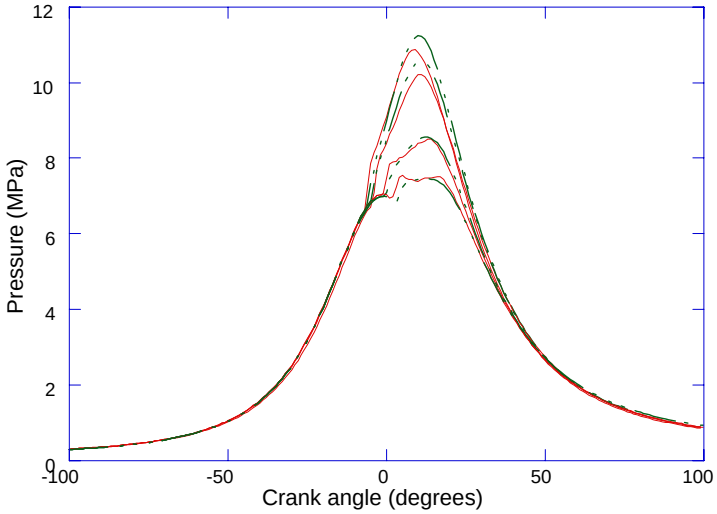

Fig. 6.9 Computed (dashed) and measured (solid) pressure data for Caterpillar engine with different injection timings: (from top) -15, -13, -8 and -5 (Kong et al., 1995).

The agreements between the measured and predicted engine-out NOx and soot trends shown in Fig. 6.10 are also very encouraging. Recent work has shown that soot emissions are somewhat under-predicted at very retarded timings, and work is in progress on improved emissions models (Hampson and Reitz, 1995).

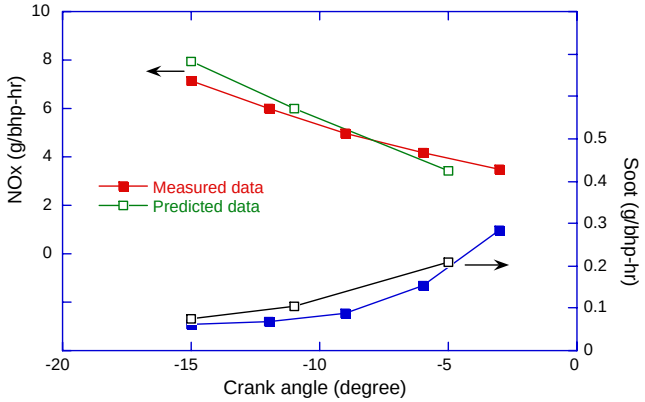

Fig. 6.10 Computed (open symbols) and measured (solid symbols) soot-NOx trade-off trend (Kong et al., 1995, Patterson et al., 1994).

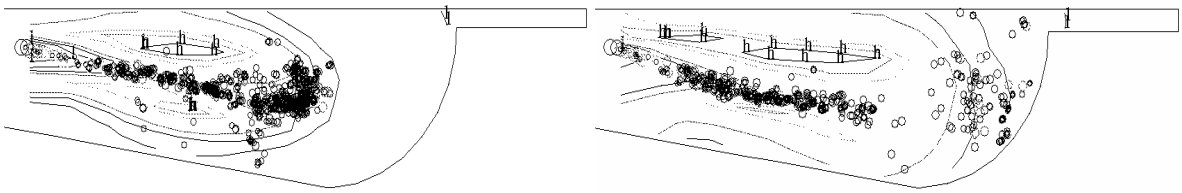

TDC h=2400K l=940K 5 ATDC h=2420K l=942K

Fig. 6.11 In-cylinder temperature contours and spray drop distribution for Tacom engine Case 1 (ϕ=0.5) at 0 and 5 degrees ATDC.

Figure 6.11 shows the predicted spray and temperature fields in the Tacom engine using the same model as used for the Caterpillar results. Notice that the orientation of the fuel spray is such that no strong wall impingement is observed, and the engine has a much smaller displacement than the Caterpillar engine (see Table 6.1). The computed and measured pressure data are shown in Fig. 6.12a, and are seen to agree very well for both engine loads considered.

The computed in-cylinder NO evolutions are also compared to the measured data as shown in Fig. 6.12b. The agreement is very good. Both experimental and computed results show that the majority of NO is formed during the diffusion burning phase and the reactions freeze during the later part of combustion.

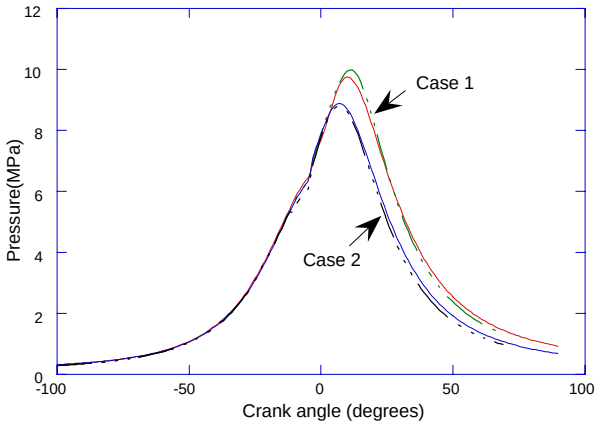

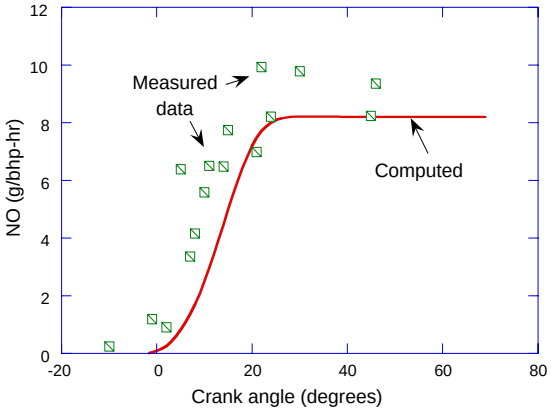

Fig. 6.12 (a.) Computed (dashed) and measured (solid) pressure data for Tacom engine Case 1 (ϕ=0.5) and Case 2 (ϕ=0.3).

(b.) Computed and measured NO evolution data for Tacom engine Case 1 (ϕ=0.5) (Kong et al., 1994).

The above results show that the use of the updated version of KIVA-II gives reasonably good agreement between measured and predicted engine

cylinder pressures and heat release rate data. It was possible to apply the same model (with the same set of model constants) to two quite different engine designs. The results show that the combustion is controlled by the details of the spray model. In particular, drop breakup and drop drag effects govern the penetration and mixing of vaporizing sprays under diesel engine conditions. The effects of spray wall impingement and enhanced drop breakup were also found to be important. The Shell model gives good predictions of diesel ignition, and the study also indicates that combustion can be modeled adequately when both laminar chemistry and turbulent mixing are incorporated in the combustion model. The present soot and NOx predictions are also encouraging. However, further testing of the combustion and emissions model performance is needed at other engine operating conditions.